Journal of Science: Advanced Materials and Devices 9 (2024) 100723

Contents lists available at ScienceDirect

Journal of Science: Advanced Materials and Devices

journal homepage: www.elsevier.com/locate/jsamd

Sustainable and cost-effective edge oxidized graphite/PEDOT:PSS nanocomposites with improved electrical conductivity

Giuseppe Greco [a], Antonella Giuri [b,*], Salvatore Gambino [b], Sonia Carallo [b], Silvia Colella [c], Chiara Ingrosso [d], Aida Kiani [e], Maria Rosaria Acocella [e], Aurora Rizzo [b], Carola Esposito Corcione [a]

[a] Università del Salento, Via per Monteroni, Km 1, I-73100, Lecce, Italy
[b] CNR-NANOTEC-Istituto di Nanotecnologia, Polo di Nanotecnologia, c/o Campus Ecotekne, Via Monteroni, I-73100, Lecce, Italy
[c] CNR NANOTEC Bari, c/o Dipartimento di Chimica, Universita' di Bari, Via Orabona 4, 70126, Bari, Italy
[d] CNR-IPCF Istituto per i Processi Chimico-Fisici, Sez. Bari, c/o Dip. Chimica, Via Orabona 4, 70126, Bari, Italy
[e] Department of Chemistry and Biology and INSTM Research Unit, Università di Salerno, Fisciano, SA, Italy

ARTICLE INFO

Keywords:
Edge oxidized graphite
PEDOT:PSS
Nanocomposites
Sustainability
Solvent-free doping
Thin films

ABSTRACT

Poly(3,4-ethylenedioxythiophene): polystyrene sulfonate (PEDOT:PSS) is a soft and conjugated polymer whose conductive properties can be properly tuned through doping with various additives or solvents, preserving its excellent processability. In this work PEDOT:PSS was combined with a cost-effective graphite derivative named Edge Oxidized Graphite (EOG) for developing a nanocomposite with improved electrical conductivity, with respect to the pristine PEDOT:PSS, through an easy and environmentally friendly doping process. Firstly, the EOG powders, produced by a green oxidation process of graphite, were deeply characterized through Fourier transform infrared (FT-IR), Thermogravimetric (TGA), and Wide-angle X-ray scattering (WAXD) analysis, showing that this nanofiller has oxygenated functional groups on the sheet edges. The quality and the stability of the EOG dispersions within PEDOT:PSS were investigated at different carbon-filler concentrations, up to high loading of 25 %wt/V of EOG through rheological analyses, demonstrating pseudo-plastic behavior and excellent long-term stability of the inks due to the absence of inhomogeneities and aggregates over time; in fact, the same inks were tested under the same rheological conditions after 21 days, showing the same viscosity trend for all EOG concentrations (%wt/V). Transmission electron microscopy (TEM) and (Scanning Electron microscopy) SEM investigation of spin-coated samples onto glass substrates were performed to morphologically evaluate the nanocomposites and estimate the average size of the sheets, particularly the mean length of 1.2 μm and an approximated thickness of 26 nm of the EOG sheets dispersed into the polymer matrix (PEDOT:PSS) was determined, while WAXD analysis allowed to identify the average layer number of the EOG sheets, obtaining thus, a direct measurement of the EOG sheets aspect ratio equal to 45. Finally, sheet resistance tests showed that the increasing concentration of EOG leads to a significant improvement in the electrical conductivity of the nanocomposites, from 1.1 S/cm for pristine PEDOT:PSS to 21.9 S/cm for nanocomposites with the highest EOG content (25 %wt/V). This work demonstrates the successful development of nanocomposite based on PEDOT:PSS doped with carbon-based filler synthesized through a green and cost-effective process, promoting their use in the production of bio/electrochemical sensors or optoelectronic devices.

1. Introduction

Over the last few years, great research efforts have been carried out on the development of polymer-based nanocomposites with different functionalities for the specific applications in the field of opto- and bio-electronics [1–3], in particular for (bio)- and electrochemical sensors [4–6], solar cells [7,8], supercapacitors [9–12], fuel cells [13,14], H_2 storage [15–17], transistors [18], etc. The use of graphite and its derivatives has rapidly increased due to their outstanding physicochemical, electrical, mechanical, and thermal properties. These materials are

Peer review under responsibility of Vietnam National University, Hanoi.
* Corresponding author.
E-mail address: antonella.giuri@nanotec.cnr.it (A. Giuri).

https://doi.org/10.1016/j.jsamd.2024.100723
Received 10 January 2024; Received in revised form 5 April 2024; Accepted 12 April 2024
Available online 16 April 2024

often used as carbon-fillers of several epoxy resins [19–22] as polymer matrices, and above all, the conductive polymers, obtaining highly-performance nanocomposites for cutting-edge applications [23–25]. Among all the classes of polymers, conjugated polymers have gained particular interest because, due to the typical molecular structure with σ single bonds alternating with π double bonds, they are characterized by electrons weakly held in the backbone and by weak π bonds that allow delocalization and free movement of electrons [26]. Different conductivity values can be reached as a function of the chemical structure and doping state [27,28]. Among conjugated polymers, poly(3,4 ethylenedioxythiophene): polystyrene sulfonate (PEDOT:PSS) received significant interest from the scientific community owing to its water solubility, good film-forming properties, high transparency, and excellent processability [29–31]. Particularly, it is made up of two monomers: poly(3,4-ethylenedioxythiophene) (PEDOT), derived from polythiophene, which carries positive charges, and polystyrene sulfonic acid (PSS), which carries negative charges on the deprotonated sulfonyl groups [29]. PSS is the most commonly used counterion, allowing the synthesis of a stable aqueous dispersion form, but due to its insulating nature, it strongly influences the electrical properties of PEDOT, which are highly dependent on the PEDOT/PSS ratio.

Many efforts, such as several solvent post-treatment and filler doping, have been investigated to improve the conductive properties of PEDOT:PSS. Solvents like diethylene glycol (DEG), dimethylsulfoxide (DMSO) and ethylene glycol (EG) can well remove PSS from the PEDOT:PSS structure by dissolving it, resulting in enhancing charge transfer between the closer PEDOT chains. However, even if the solvent post-treatment is simple, it can affect the surface of the sample and reduce the stability of the performance [32–35].

Concerning the filler doping, the use of carbon-based fillers as secondary dopants for PEDOT:PSS to develop a composite with restored or improved conductivity properties is widespread due to the synergistic effect induced by the interfacial contact between the great specific surface areas of the carbon materials and PEDOT:PSS polymers, that improves the performances [36].

In this context, several carbon-based materials from graphite with different dimensionality and functionalization (i.e., graphene, graphene oxide (GO), reduced graphene oxide (rGO), chemically functionalized graphene oxide (fGO)) to carbon nanotubes (CNTs), up to the less noble carbon filler derived from waste (i.e., carbon ashes, carbon black etc.) were used to develop nanocomposites with high performance for the most disparate applications [8,10–12,37]. In particular, the choice of using graphite-based fillers is strictly related to their excellent properties, for example, graphene is an attractive nanofiller owing to its high intrinsic charge mobility (200 000 $cm^2 V^{-1} s^{-1}$), a high current density of 108 A cm^{-2}, a large surface area (2630 $m^2 g^{-1}$), thermal conductivity of ≈5000 W $m^{-1} K^{-1}$, an elastic modulus of ≈1.0 TPa, and optical transmittance of ≈97.7% [38]. However, recent studies show that graphene is a 2D material with 3D deformation [39] that exhibits hydrophobicity, making it unstable in an aqueous medium. To address this problem, graphene can be functionalized with oxygen-containing functionalities to form GO that is hydrophilic and water-soluble but less conductive than pure graphene. Therefore, GO is reduced through chemical [40,41] or thermal treatment [42,43] to produce rGO [44], which exhibits higher conductivity than GO. The level of electrical conductivity achieved in rGO is directly proportional to the degree of reduction of GO. With a high degree of reduction, rGO exhibits properties similar to pure graphene, but with some structural defects, depending on the reducing agent and the experimental conditions employed [45].

The inclusion of these graphitic fillers into a proper polymer matrix allows the development of composite materials with excellent properties resulting from the combination and possibly interaction between the two.

In particular, regarding the inclusion of graphitic fillers into PEDOT:PSS, Chang et al. [46] have reported other solutions, which include the fabrication of transparent, low-temperature, flexible PEDOT:PSS/graphene nanocomposites for electrodes using a solution-based technique. To further simplify the manufacturing process of PEDOT:PSS/graphene nanocomposite, Soltani-Kordshuli et al. [47], have developed a novel, controllable, and scalable ultrasonic substrate vibration-assisted spray coating method to produce a high-performance hybrid graphene-PEDOT:PSS film. Kim et al. [30] developed high performance thermoelectric PEDOT:PSS/graphene nanocomposite thin films with a small amount of graphene and a high level of carrier mobility; while Mahakul et al. [48] coupled the use of CNT and rGO to produce hybrid nanocomposites with improved conductivity for transparent electrode applications. Seol et al. [49] developed PEDOT:PSS-based nanocomposites with enhanced conductivity by incorporating functionalized-rGO fillers for producing stretchable transparent conducting electrodes.

The reduction of GO ex-situ and after inclusion into PEDOT:PSS by means of different green reducing agents, such as UV irradiation or glucose (G), has been widely investigated by Giuri et al. for photovoltaic applications [7,8]. Moreover, they demonstrated that glucose can be an effective green dispersing/reducing agent to produce G-GO-PEDOT:PSS ternary nanocomposite films by drop casting technique into a silicone mold, resulting in a flexible thin film for supercapacitor applications [10,50]. Recently, they developed an innovative method for recycling carbon-based ashes waste, using them as fillers of electrically conductive PEDOT:PSS-based inks suitable for the fabrication of supercapacitors [11,51]. While the use of a waste product contributes to a change of mindset towards a circular economy model, the heterogeneity of the waste product itself is a limiting factor in achieving positive bio-electronic properties. Therefore, the use of a commercial GO, as reported in our previous work [12], seemed to be a more suitable choice to achieve the tightening properties that bio- and optoelectronic applications require.

Generally, solution processing techniques such as drop-casting [52], spin coating [53], spray coating [54], inkjet printing [55], and aerosol jet printing [11,12] have been successfully used for fabricating PEDOT:PSS based thin films in biosensors and flexible electronic devices.

Starting from the promising results on PEDOT:PSS increased conductivity, specific capacitance, stability, and film-forming properties [7,10,11]; in this paper the inclusion of a new green carbon-filler Edge Oxidized Graphite (EOG) into PEDOT:PSS has been explored for developing nanocomposites with increased electrical conductivity. EOG was obtained through a simple, sustainable and cost-effective process, by functionalizing high surface area graphite (HSAG) in presence of an excess of hydrogen peroxide (H_2O_2), acting as reactant and solvent in the absence of a catalyst [56].

The functional groups of the synthesized filler were evaluated by FT-IR, TGA, and WAXD analyzes to better understand the characteristics of EOG and optimize the process conditions for the nanocomposite development. Several EOG concentrations, from 0 to 25 %wt/V, have been explored and characterized by a rheological, morphological, and electrical point of view for better understanding the interaction between the two components of the nanocomposite and the influence of the filler inclusion on the PEDOT:PSS properties, for possible applications as bio/electrochemical sensors or optoelectronic devices.

2. Experimental

2.1. Materials

PEDOT:PSS aqueous dispersion (Clevios™ PH 1000) was purchased by Heraeus with 1.0–1.3 %wt PEDOT:PSS concentration and the typical PEDOT:PSS ratio of 1:2.5 w/w. It appears as a dark blue liquid, completely miscible in water with 850 S/cm of specific conductivity, measured on the dried coating after the addition of 5% Dimethyl sulfoxide and 15–60 mPa s of viscosity range as reported in its technical data sheet [57]. PEDOT:PSS was used as received without any further

purification process.

Edge Oxidized Graphite (EOG) was prepared by a green method with hydrogen peroxide [56], which simplifies exfoliation and turns it into powder form. The preparation procedure is explained in detail below.

High surface area graphite (HSAG), with a minimum carbon of 99.5 %wt and a surface area of 330 m^2/g, was purchased from Asbury Graphite Mills Inc. and HSAG oxidation has been obtained by hydrogen peroxide. HSAG (500 mg) and H_2O_2 (500 mL) were introduced in a 1 L flask and placed in a thermostat bath at 60 °C, under magnetic stirring. After 24 h, about 1 L of water was added, the whole was centrifugated and finally, the isolated pellet was dried at 60 °C overnight.

2.2. Edge Oxidized Graphite (EOG) characterization

Surface areas of the graphite sample were measured by nitrogen adsorption at liquid nitrogen temperature (77 K) with a NOVA Quantachrome 4200e instrument. Before adsorption measurements, the samples were degassed at 60 °C under vacuum for 24 h.

The surface area values were determined by using an 11-point Brunauer–Emmett–Teller (BET) analysis. Elemental analysis was performed with a Thermo FlashEA 1112 and evaluated by a CHNS–O analyzer after pre-treating the samples in an oven at 100 °C for 12 h.

Fourier transform infrared (FT-IR) spectra were obtained with a FT-IR (BRUKER Vertex70) spectrometer equipped with a deuterated triglycine sulphate detector and a KBr beam splitter, at a resolution of 2.0 cm^{-1}. The frequency scale was internally calibrated to 0.01 cm^{-1} using a He–Ne laser. 32 scans were averaged to reduce the noise. Spectra of powder samples have been collected by using KBr pellets.

Thermogravimetric analysis (TGA) was carried out on TA Instruments Q500, from room temperature up to 800 °C at a heating rate of 10 °C/min, under N_2 flow of 60 mL/min.

Wide-angle X-ray diffraction (WAXD) patterns were obtained by an automatic Bruker D2 phaser diffractometer, in reflection, at 35 KV and 40 mA, using nickel-filtered Cu Kα radiation (1.5418 Å). Correlation lengths (D) were determined by using Scherrer's equation (Eq. (1)):

$$D = \frac{K\lambda}{\beta \cos \vartheta} \quad (1)$$

where λ is the wavelength of the incident X-rays, β is the line broadening at half the maximum intensity, after subtracting the instrumental line broadening, in radians, and θ is the diffraction angle, assuming the Scherrer constant K = 1.

Bragg's law (Eq. (2)) and Scherrer equation (Eq. (1)) were used to determine the interlayer spacing and the crystal size of EOG, respectively. Taking into account the crystal size evaluated on the higher reflection (002) and the d_{002} interlayer distance, the average layer number of the EOG stacks dispersed in the PEDOT:PSS was evaluated

$$n\lambda = 2dsen(\theta) \quad (2)$$

WAXD analysis was performed on EOG powders and on liquid EOG-water formulations drop-casted onto glass substrates and thermally annealed at 120 °C for 20 min to evaluate the EOG solubility and exfoliation in water and optimize the inks preparation. EOG-water solutions non-sonicated, sonicated, and extremely diluted with water were analyzed and compared with pristine EOG. This analysis showed us that the best method to prepare the inks is described below.

2.3. EOG/PEDOT:PSS inks preparation

Firstly, PEDOT:PSS aqueous solution was sonicated into an ultrasonic cleaner for 10′ minutes and filtered by PVDF filter (0.45 μm), then EOG, in several concentrations, was weighted through BEL Engineering M5-HPB-105i-ION balance and directly added into PEDOT:PSS aqueous solution; the mixture was magnetically stirred at 700 rpm and room temperature (RT) for 60' min and the influence of EOG was evaluated by preparing several EOG/PEDOT:PSS dispersions (0.2, 1, 5, 10, 15, 20, and 25 %wt/V). Each solution developed is labeled as reported in Table 1.

2.4. EOG/PEDOT:PSS inks characterization

The rheological analysis of the liquid formulations was performed using a Malvern Kinexus Pro + strain-controlled rheometer equipped with a parallel plate geometry (radius = 12.5 mm) in steady state mode with 0.4 gap and a shear rate range from 0.1 to 1000 s^{-1} at RT. All solutions were tested just after being prepared and after 21 days, and each test was repeated at least three times to check the repeatability of the results.

The stability of the formulations was assessed qualitatively by taking photographs of the solutions on day 0 and after 21 days of storage in air.

2.5. Thin films of EOG/PEDOT:PSS nanocomposites preparation and characterization

TEM analyses were performed by using a Jeol Jem-1011 microscope operating at 100 kV and equipped by a high-contrast objective lens, with a W filament as an electron source, and an ultimate point resolution of 0.34 nm. Images were acquired by a Quemesa Olympus CCD 11 Mp Camera. Samples were prepared by drop-casting 3 μl of the samples onto 300 mesh amorphous carbon-coated Cu grids, spinning at 9000 rpm for 1 min. Size statistical analysis of the EOG sheets was performed by using the freeware ImageJ analysis program.

All nanocomposites were spin-coated using a Laurell 650 M Spin Coater and depositing 100 μl at 2000 rpm for 40 s onto glass substrates (3 × 3 cm) in air. After deposition, the thin films were thermally annealed at 120 °C for 20 min on a hot plate. The substrates were previously cleaned with detergent solutions (deionized water, acetone, and isopropanol solvents) in an ultrasonic cleaner for 10' min for each step and their surfaces were hydrophilized by a 20′ min UV/Ozone treatment using the UV/Ozone ProCleanerTM Plus.

SEM images of spin-coated nanocomposite were acquired with a FESEM microscope Zeiss Sigma 300 VP, using a GEMINI technology and an applied acceleration voltage of 5 and 10 kV.

The thickness of all the spin-coated films was measured using a D-120 KLA Tencor stylus profiler.

Sheet resistance measurements of EOG/PEDOT:PSS thin films on glass were performed in air and at RT conditions using an Ecopia 3100 system in the van der Paw configuration where gold tips were placed on the four corners of squared samples (1.5 × 1.5 cm).

3. Results and discussion

3.1. Edge oxidized graphite characterization

The EOG was fully characterized by elemental analysis, FT-IR, TGA, and WAXD. As previously reported [56] the oxidation is effective after 24 h providing the EOG powder with an O/C ratio of 0.11. The FT-IR spectroscopy analysis shown in Fig. 1a revealed the nature of the functional groups introduced by this oxidation procedure in comparison

Table 1
EOG content and ID of the developed nanocomposites.

PEDOT:PSS V [μL]	EOG wt [mg]	Nanocomposite ID
500	0	PEDOT:PSS
500	1	EOG (0.2%)/PEDOT:PSS
500	5	EOG (1%)/PEDOT:PSS
500	25	EOG (5%)/PEDOT:PSS
500	50	EOG (10%)/PEDOT:PSS
500	75	EOG (15%)/PEDOT:PSS
500	100	EOG (20%)/PEDOT:PSS
500	125	EOG (25%)/PEDOT:PSS

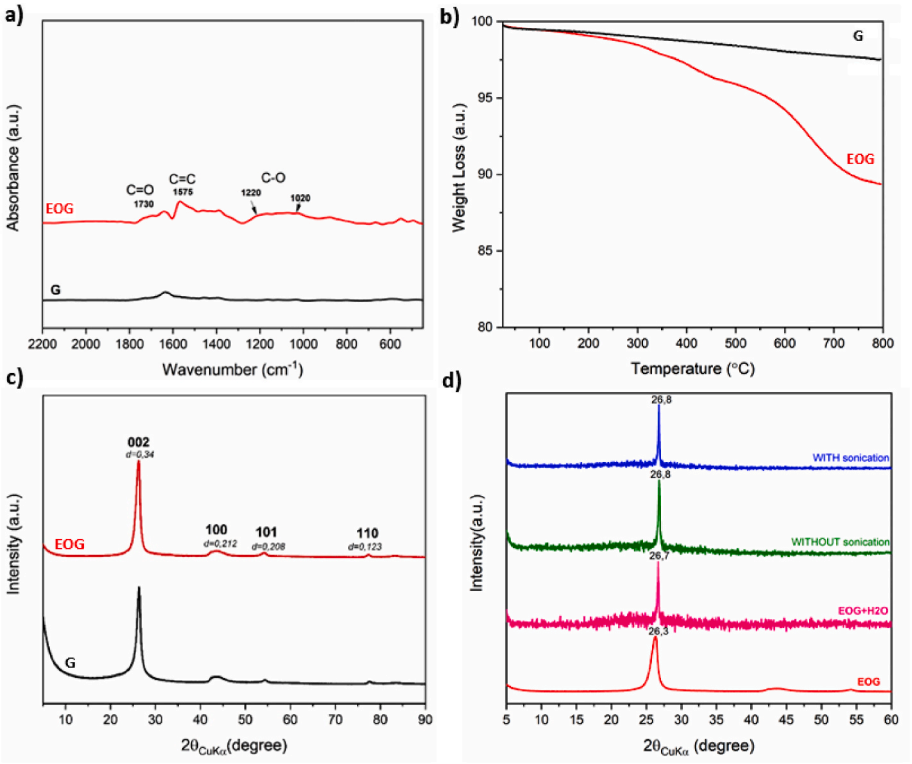

Fig. 1. a) Comparison of FT-IR spectra b) TGA scan and c) WAXD patterns between G (black) and EOG (red). d) Comparison of WAXD patterns of EOG/water solution ultrasonicated, non-ultrasonicated and extremely diluted with pristine EOG.

with the pristine graphite used as the starting material. As a result, the appearance of a band at 1730 cm^{-1} is in agreement with the introduction of carbonyl groups, mainly carboxyl, as well as the broad band in the region 1220-1020 cm^{-1}, related to the stretching of C–O single bonds. In addition, the peak centered at 1575 cm^{-1} is attributed to the C═C stretching that is shifted with respect to graphite (G) (1630 cm^{-1}) and increases in intensity due to oxidation.

The TGA scans of G and EOG in Fig. 1b show minimal variations in thermal degradation, with an increased weight loss percentage for EOG, indicating an increased degree of oxidation.

More interestingly is the WAXD pattern after the oxidation procedure (Fig. 1c). Specifically, the maintenance of 002 reflection after oxidation with d = 0.34 nm, reveals an unchanged interlayer distance due to the presence of the oxygen functionalities on the edge of the graphitic planes rather than between the layers. As the π-system of graphite has not been altered, this feature is crucial for the possible electric properties of this filler. Moreover, the 002 peak becomes narrower after the oxidation possibly due to the removal of an amorphous component as previously reported [56].

Furthermore, as reported in Fig. 1d, the presence of water, used to disperse the EOG sheets before dispersing them in the PEDOT:PSS aqueous solution, in the initial procedure, seems to remove the exfoliated part of EOG and recompose the graphitic structure, because the reflection 002, characteristic of the order perpendicular to the plane, becomes narrower and shifts slightly to the right both with and without sonication process. The reflections, on the other hand, relating to the structure between 40 and 45° theta are not visible, probably because the film is too thin, and the amount of sample is not sufficient.

This analysis showed that the best way to preserve the exfoliated part of the EOG sheets is to add it directly into the polymer (PEDOT:PSS), rather than pre-mixing the EOG in distilled water before dispersing it in PEDOT:PSS, so this is the procedure adopted for making the nanocomposite.

3.2. Characterization of EOG/PEDOT:PSS inks rheological analysis

The viscosity of pristine PEDOT:PSS as a function of the shear rate (ranging from 0.1 to 1000 s^{-1}) was compared with that of PEDOT:PSS mixed with different EOG concentrations (0.2, 1, 5, 10, 15, 20 and 25 % wt/V) as reported in Fig. 2b,c,d,e,f,g and h. Each investigated solution has shown a pseudo-plastic behavior; therefore, the viscosity decreases as the shear rate increases. Particularly, the addition of a small amount of EOG (0.2, 1, and 5 %wt/V) does not seem to change the viscosity of the solutions compared to pure PEDOT:PSS, over the entire shear rate range analyzed, that is around 1.15 Pa s at the lower shear rate (0.1 s^{-1}) and 0.013 Pa s at the highest (1000 s^{-1}). Instead, after adding the EOG in 10 and 15 %wt/wt, the viscosity of the PEDOT:PSS increases above all, in the entire investigated shear rate range, passing to 1.65 Pa s at 0.1 s^{-1} and 0.025 Pa s at 1000 s^{-1}. However, the highest increment of viscosity (2.03 Pa s at 0.1s^{-1} and 0.037 Pa s at 1000s^{-1}) is reached after adding the 25 %wt/V of EOG, probably due to the interaction between the functional groups of EOG and PEDOT:PSS polymer chains [20]. The stability of the developed formulations was qualitatively assessed by taking photographs of the inks immediately after preparation and after 21 days, as shown in insets of Fig. 2. The pictures were analyzed to check for any inhomogeneities or aggregates, and none were found, indicating that the inks remained stable after 21 days. To further validate the above, the same solutions were tested again from a rheological point of view after 21 days under the same conditions. The results showed that the viscosity curves have the same trend for all EOG concentrations (% wt/V) used, indicating that the viscosity values of the solutions did not change over time. Therefore, the inks have excellent long-term stability.

3.3. EOG/PEDOT:PSS nanocomposites film characterization

The effectiveness of the nanocomposite development was demonstrated through the combination of morphological and physical techniques, such as SEM and TEM with WAXD, on thin film deposited by spin

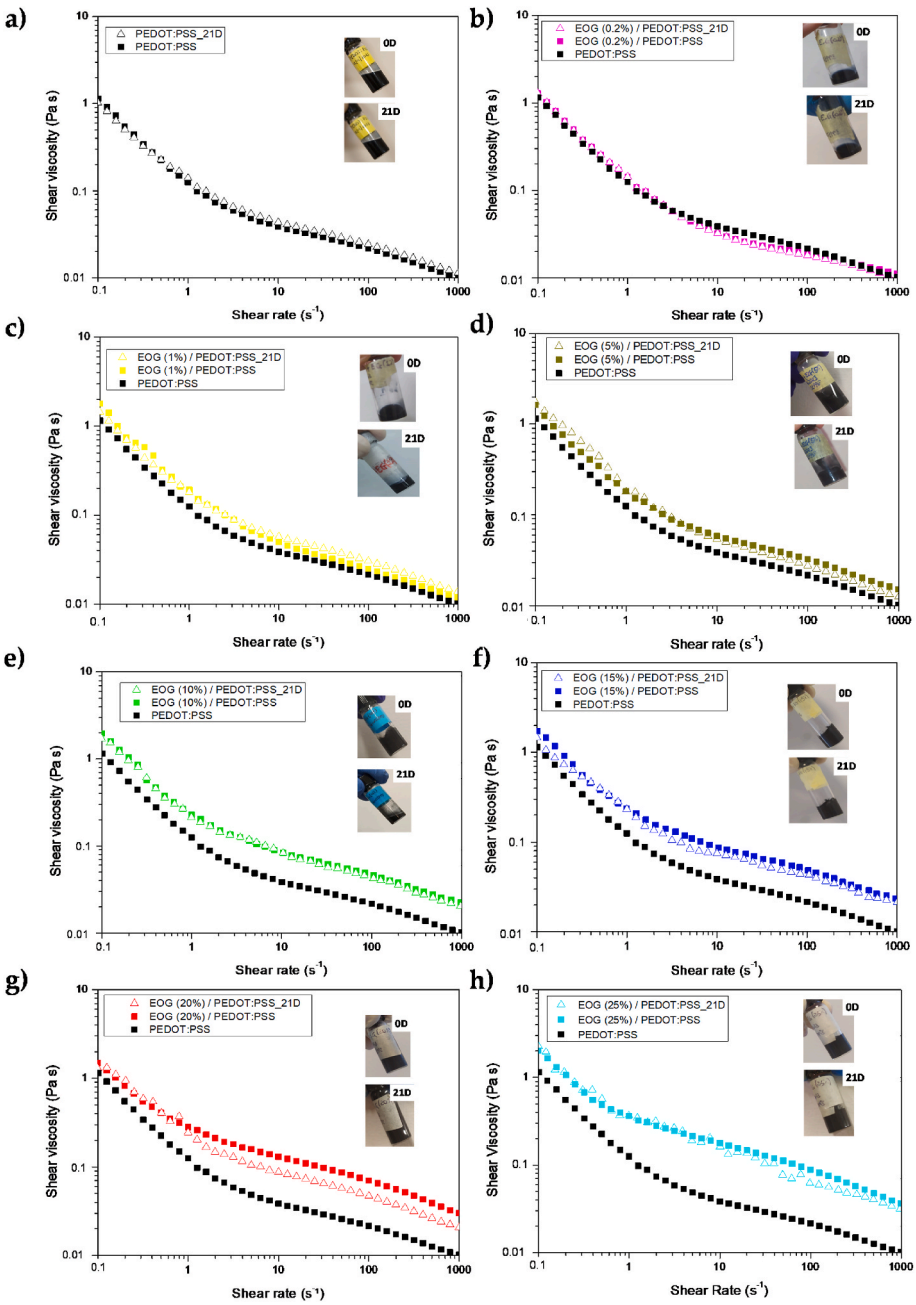

Fig. 2. Rheological behavior of PEDOT:PSS based inks, at day 0 and 14, without (a) and with b) EOG (0.2%); c) EOG (1%); d) EOG (5%); e) EOG (10%); f) EOG (15%); g) EOG (20%); h) EOG (25%).

coating, whose results were reported respectively in Figs. 3 and 4.

It is visually evident that a homogeneous darkening of the film by increasing the amount of EOG in the polymer matrix, as reported in Fig. 3a. Particularly, SEM analysis evidenced a good and homogeneous dispersion of the EOG sheets within the PEDOT:PSS. Indeed, Fig. 3b shows the morphology of a pristine PEDOT:PSS film having a uniform surface, while Fig. 3c and d shows a clear distribution and interconnection of irregularly shaped EOG sheets among each other, with 15 and 25 %wt/V of EOG/PEDOT:PSS, respectively.

An in-depth analysis of the nanocomposite was carried out by combining the high-resolution technique of TEM with WAXD. In Fig. 4 (a,b) TEM micrographs of the nanocomposite containing the 25% EOG have been reported, showing EOG flakes of irregular morphology with a wide range of sizes from hundreds of nanometers to 2.5 μm and exhibiting an inhomogeneous image contrast. The latter is reasonably due to sheets overlapping in multilayers, which originates from aromatic π-π stacking interactions among sheets, as well as chemisorption of PEDOT:PSS onto the EOG basal plane. As evidenced by WAXD spectra of the most concentrated nanocomposites (20 and 25 %wt/V) reported in Fig. 4c,d, together with the characteristic 002 reflection of the graphite, there is an increased amorphous band that can be attributed both to the PEDOT:PSS and to the exfoliated EOG homogeneously distributed into the polymer [53,58].

The results obtained by TEM and WAXD characterizations were combined to calculate the aspect ratio of the EOG sheets dispersed within the PEDOT:PSS, as further confirmation of the nanocomposite formation. In detail, the characteristic mean size of the sheets (average length) were estimated using the freeware ImageJ analysis program on TEM images of EOG (25%)/PEDOT:PSS nanocomposite and the interlayer spacing was calculated from the WAXD spectra of the most

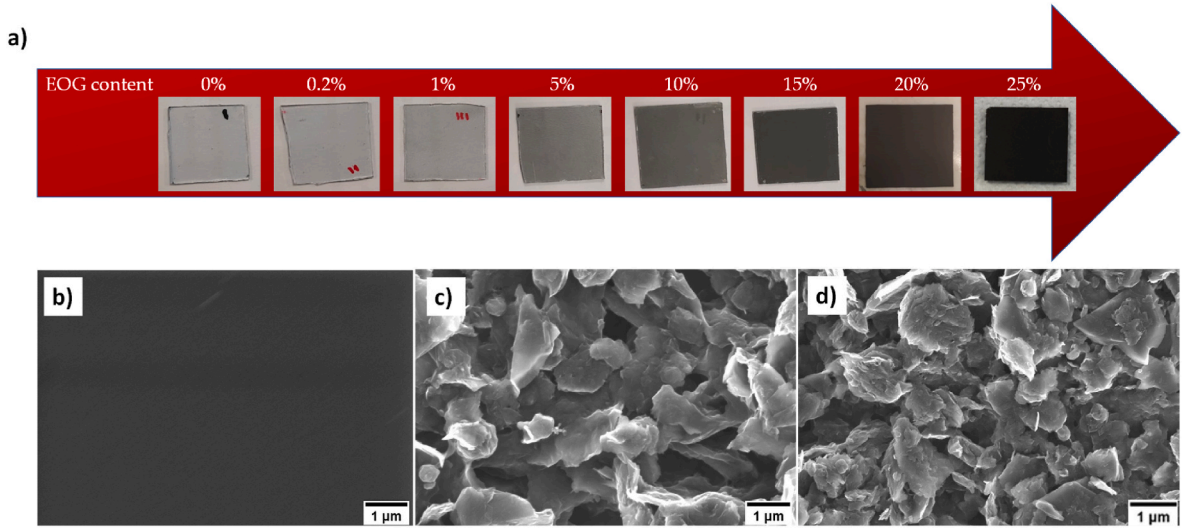

Fig. 3. a) Thin films developed through spin-coating deposition of all liquid formulations, b) SEM image of spin-coated pristine PEDOT:PSS; c) SEM image of spin-coated EOG (15%)/PEDOT:PSS; d) SEM image of spin-coated EOG (25%)/PEDOT:PSS.

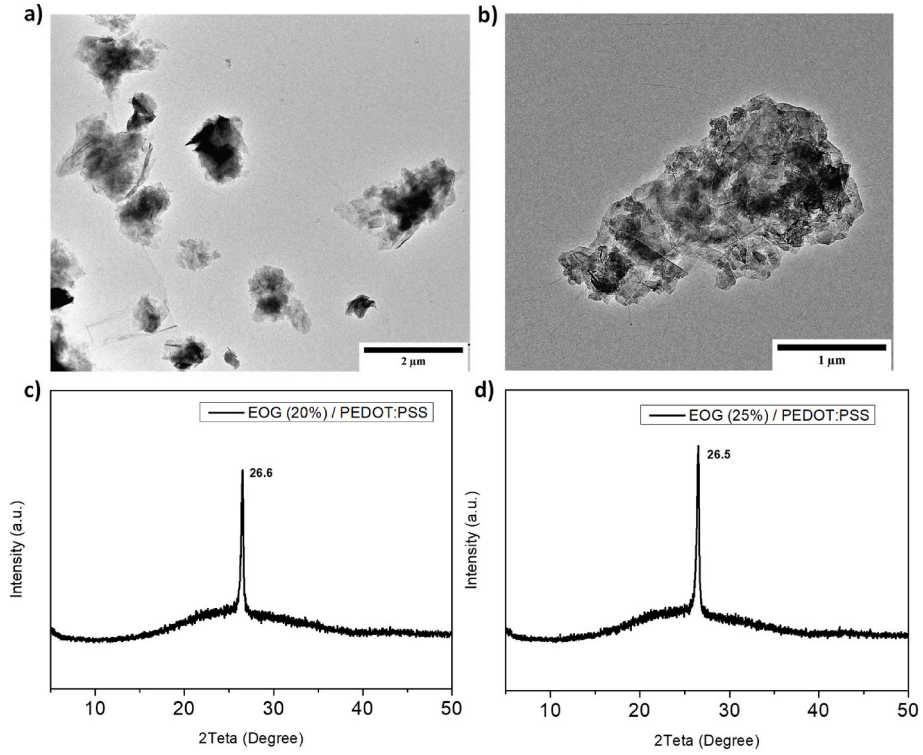

Fig. 4. a)-b) TEM images of EOG sheets dispersed into PEDOT:PSS with a concentration of 25%, at different magnifications (5kx and 10kx); c)-d) WAXD spectrum of the most concentrated solutions (EOG (20%)/PEDOT:PSS (c) and EOG (25%)/PEDOT:PSS (d)).

concentrated nanocomposites (20 and 25 %wt/V). More specifically, an average layer number of 77 and a mean length of 1.2 µm of the EOG sheets dispersed into the polymer matrix (PEDOT:PSS) was determined, showing an aspect ratio value of 45 with an approximated thickness of 26 nm. The high aspect ratio value indicates good intercalation of EOG sheets among PEDOT:PSS polymer chains. Hence, the obtained results, in agreement with the data obtained from the EOG synthesis in the previous work [56], confirm the formation of a nanocomposite with graphite edge homogeneously distributed in the PEDOT:PSS, further validating the effectiveness of the developed approach. Furthermore, the possible connection between the carboxyl groups on the edges of the layers through hydrogen bonds may promote an increase in electrical conductivity.

3.4. EOG/PEDOT:PSS nanocomposites electrical characterization

In Table 2 we reported the experimental data on the sheet resistance (R_s) of EOG/PEDOT:PSS films against EOG concentration (%wt/V) compared with the reference sample (PEDOT:PSS). Pristine PEDOT:PSS shows an $R_s = 1.3*10^5$ (Ω/sq), which is consistent with previously reported results for as-prepared PEDOT:PSS films from PEDOT:PSS aqueous solution [59]. However, it is worth noting that for bio and

Table 2
Sheet resistance, thickness, resistivity, and conductivity of all nanocomposites.

EOG %wt/V	0	0.2	1	5	10	15	20	25
Sheet resistance [Ω/sq]	$1.3*10^5$	$1.1*10^5$	$7.6*10^4$	$1.4*10^4$	$2.7*10^3$	$6.4*10^2$	$4.9*10^2$	$3.8*10^2$
Thickness [cm] •10-7	70	65	70	175	500	900	1100	1200
Resistivity [Ωcm]	0.91	0.72	0.53	0.25	0.14	0.06	0.05	0.04
Conductivity [S/cm]	1.1	1.4	1.8	4.1	7.4	17.4	18.6	21.9

optoelectronic applications, usually, its conductivity is enhanced by orders of magnitude by adding dimethyl sulfoxide (DMSO) or ethylene glycol (EG) into the aqueous solution [60–63], which are typically non-green chemical agents or by incorporating carbon fillers such as CNT [64], rGO [48], and fGO [49] whose production process is time-consuming and expensive.

In the present study, the measured R_s of each film was found to be strongly dependent on the EOG content in the nanocomposite as shown in Fig. 5a. For an EOG concentration lower than 1 %wt/V there is a negligible variation of the film's sheet resistance, but as the EOG concentration increases further, the sheet resistance decreases down to 3 orders of magnitude as we move up to 25 %wt/V of EOG. The addition of EOG into the matrix with a concentration of 25 %wt/V results in a composite film sheet resistance of $3.8*10^2$ (Ω/sq) that is comparable to that of DMSO (5%) doped PEDOT:PSS, whose measured R_s turned out to be of $2*10^2$ (Ω/sq). This result is consistent with films morphology studied in the previous section, in which the EOG leaflets intertwine among themselves and with the polymer chains of PEDOT:PSS, generating strong interconnections that allow the movement of weakly retained electrons in the backbone and π-bonds of the PEDOT:PSS chains. Therefore, the increase in EOG concentration has led to a stronger interconnection between EOG leaflets themselves and with PEDOT:PSS polymer chains, as shown in Fig. 3b-d.

We also calculated the DC electrical resistivity and conductivity according to the following equation [65,66]:

$$\sigma = \frac{1}{\rho} = \frac{1}{R_s * d} \tag{3}$$

where σ is the electrical conductivity, ρ is the resistivity and d the sample thickness. From the analysis of Fig. 5 we can clearly see that both the sheet and the bulk resistance tend asymptotically to a minimum value for an EOG concentration larger than 10 %wt/V. Furthermore, to verify that this asymptotic value is a key feature of our EOG-based composite, we performed sheet resistance measurements on two other nanocomposites based on different formulas of PEDOT:PSS (Clevios 4083 and Sigma-Aldrich). Figure S1 shows that although pristine PEDOT:PSS films are characterized by different sheet resistance values, all of them have similar values once doped with the same amount of EOG.

4. Conclusion

The present work shows the successful development of a conductive nanocomposite based on EOG/PEDOT:PSS through a sustainable, cost-effective and highly reproducible process. Compared with the other more expensive carbon based fillers used in literature, the EOG used in this work is produced through a green, and cheap oxidation process of graphite, resulting in the formation of oxygenated functional groups only on the sheet edges rather than within the sheet or between the layers. These oxygenated functional groups allowed the inclusion and the dispersion of the carbon filler directly into the PEDOT:PSS aqueous solution through an easy and fast mixture process without using further costly steps. Rheological characterization highlights a pseudo-plastic behavior and an increase in viscosity of the EOG (25%)/PEDOT:PSS ink up to 2.03 Pa s and 0.037 Pa s at 0.1 s^{-1} and 1000 s^{-1}, respectively; furthermore, long-term stability and good dispersion of the EOG sheets within PEDOT:PSS is demonstrated because there is no significant variation in viscosity after 21 days, these are fundamental characteristics for optimizing the spin coating deposition. By means of ImageJ software applied on TEM images combined with WAXD analysis, a high aspect ratio value of 45 is calculated, evidencing a good EOG intercalation within PEDOT:PSS polymer chains and exfoliation of the EOG stacks. This results in a homogeneous distribution of EOG sheets into the PEDOT:PSS film as shown by SEM analysis. Furthermore, the sheet resistance (R_s) is strongly dependent on the EOG content, decreasing down to 3 orders of magnitude as we moved from pure PEDOT:PSS ($1.3 * 10^5$ Ω/sq) to the 25 %wt/V EOG/PEDOT:PSS nanocomposite ($3.8 * 10^2$ Ω/sq), simply using a green and environmentally friendly filler, without the use of solvents. Future developments of this work will proceed with further optimization of the preparation of the inks to improve the intercalation, exfoliation, and dispersion of the EOG sheets within the PEDOT:PSS, using green dispersing agents and aiming to a further improvement of nanocomposites electrical properties. This result is of crucial importance for producing biosensors, electrochemical sensors, and/or optoelectronic devices where adequate conductivity values are required.

CRediT authorship contribution statement

Giuseppe Greco: Formal analysis, Investigation, Visualization, Writing – original draft. **Antonella Giuri:** Conceptualization, Methodology, Supervision, Validation, Writing – review & editing. **Salvatore Gambino:** Formal analysis, Supervision, Writing – original draft, Writing – review & editing, Data curation. **Sonia Carallo:** Formal analysis. **Silvia Colella:** Formal analysis. **Chiara Ingrosso:** Data

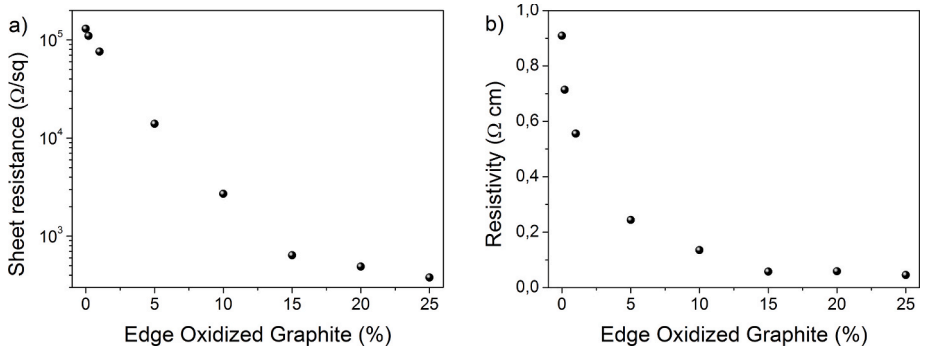

Fig. 5. Sheet resistance (a) and resistivity (b) data as a function of EOG content.

curation, Formal analysis, Supervision, Writing – original draft, Writing – review & editing. **Aida Kiani:** Investigation. **Maria Rosaria Acocella:** Supervision, Writing – original draft, Writing – review & editing. **Aurora Rizzo:** Validation. **Carola Esposito Corcione:** Conceptualization, Methodology, Project administration, Supervision, Validation.

Declaration of competing interest

The authors declare the following financial interests/personal relationships which may be considered as potential competing interests:

Giuseppe Greco reports financial support was provided by Italian MASE Ministry and Reilab srl. If there are other authors, they declare that they have no known competing financial interests or personal relationships that could have appeared to influence the work reported in this paper.

Acknowledgments

A.G and A.R. acknowledge PNRR MUR project: "Integrated Infrastructure Initiative in Photonic and Quantum Sciences" - I-PHOQS (IR0000016). A.R. acknowledge the PERMANENT project - RSH2A_000012 - funded by Italian MASE Ministry, call PNRR M2C2 INV. 3.5 RICERCA E SVILUPPO SULL'IDROGENO lettera A". S.G. acknowledges the Project "Tecnopolo per la medicina di precisione" (TecnoMed Puglia) Regione Puglia: DGR n.2117 del November 21, 2018, CUP: B84I180 0 0540 0 02' and the Project "Nano Foundries and Fine Analysis – Digital Infrastructure (NFFA-DI)" (CUP B53C22004310006), supported by the Italian Ministry of Research (MUR) in the framework of the National Recovery and Resilience Plan (NRRP), funded by the European Union – NextGenerationEU. G.G. acknowledge the funding received from the PhD scholarship: "Eco-sustainable anticorrosive coatings solutions for components in the mobility sector" co-funded by Italian MASE Ministry and Reilab srl, called PNRR, DM n. 352.

Appendix A. Supplementary data

Supplementary data to this article can be found online at https://doi.org/10.1016/j.jsamd.2024.100723.

References

[1] S. Ansari, E.P. Giannelis, Functionalized graphene sheet—poly (vinylidene fluoride) conductive nanocomposites, J. Polym. Sci. B Polym. Phys. 47 (2009) 888–897.
[2] T. Ramanathan, A. Abdala, S. Stankovich, D. Dikin, M. Herrera-Alonso, R. Piner, D. Adamson, H. Schniepp, X. Chen, R. Ruoff, Functionalized graphene sheets for polymer nanocomposites, Nat. Nanotechnol. 3 (2008) 327–331.
[3] S. Stankovich, D.A. Dikin, G.H. Dommett, K.M. Kohlhaas, E.J. Zimney, E.A. Stach, R.D. Piner, S.T. Nguyen, R.S. Ruoff, Graphene-based composite materials, Nature 442 (2006) 282–286.
[4] M.A. Eshlaghi, E. Kowsari, A. Ehsani, B. Akbari-Adergani, M. Hekmati, Functionalized graphene oxide GO-[imi-(CH2)2-NH2] as a high efficient material for electrochemical sensing of lead: synthesis surface and electrochemical characterization, J. Electroanal. Chem. 858 (2020) 113784, https://doi.org/10.1016/j.jelechem.2019.113784.
[5] A. Popov, R. Aukstakojyte, J. Gaidukevic, V. Lisyte, A. Kausaite-Minkstimiene, J. Barkauskas, A. Ramanaviciene, Reduced graphene oxide and polyaniline nanofibers nanocomposite for the development of an amperometric glucose biosensor, Sensors 21 (2021) 948.
[6] Y. Zheng, D. Lee, H.Y. Koo, S. Maeng, Chemically modified graphene/PEDOT:PSS nanocomposite films for hydrogen gas sensing, Carbon 81 (2015) 54–62, https://doi.org/10.1016/j.carbon.2014.09.023.
[7] A. Giuri, S. Masi, S. Colella, A. Kovtun, S. Dell'Elce, E. Treossi, A. Liscio, C. Esposito Corcione, A. Rizzo, A. Listorti, Cooperative effect of GO and glucose on PEDOT:PSS for high VOC and hysteresis-free solution-processed perovskite solar cells, Adv. Funct. Mater. 26 (2016) 6985–6994, https://doi.org/10.1002/adfm.201603023.
[8] A. Giuri, S. Masi, S. Colella, A. Listorti, A. Rizzo, G. Gigli, A. Liscio, E. Treossi, V. Palermo, S. Rella, C. Malitesta, C. Esposito Corcione, UV reduced graphene oxide PEDOT:PSS nanocomposite for perovskite solar cells, IEEE Trans. Nanotechnol. 15 (2016) 725–730, https://doi.org/10.1109/TNANO.2016.2524689.
[9] K. Zhang, L.L. Zhang, X. Zhao, J. Wu, Graphene/polyaniline nanofiber composites as supercapacitor electrodes, Chem. Mater. 22 (2010) 1392–1401.
[10] A. Giuri, S. Colella, A. Listorti, A. Rizzo, C. Mele, C.E. Corcione, GO/glucose/PEDOT:PSS ternary nanocomposites for flexible supercapacitors, Compos. B Eng. 148 (2018) 149–155, https://doi.org/10.1016/j.compositesb.2018.04.053.
[11] A. Giuri, R. Striani, S. Carallo, S. Colella, A. Rizzo, C. Mele, S. Bagheri, M. Seiti, E. Ferraris, C. Esposito Corcione, Waste carbon ashes/PEDOT:PSS nano-inks for printing of supercapacitors, Electrochim. Acta 441 (2023) 141780, https://doi.org/10.1016/j.electacta.2022.141780.
[12] G. Greco, A. Giuri, S. Bagheri, M. Seiti, O. Degryse, A. Rizzo, C. Mele, E. Ferraris, C. E. Corcione, Pedot:PSS/Graphene oxide (GO) ternary nanocomposites for electrochemical applications, Molecules 28 (2023), https://doi.org/10.3390/molecules28072963.
[13] B. Baruah, A. Kumar, G.R. Umapathy, S. Ojha, Enhanced electrocatalytic activity of ion implanted rGO/PEDOT:PSS hybrid nanocomposites towards methanol electro-oxidation in direct methanol fuel cells, J. Electroanal. Chem. 840 (2019) 35–51, https://doi.org/10.1016/j.jelechem.2019.03.053.
[14] B. Saner, S.A. Gürsel, Y. Yürüm, Layer-by-layer polypyrrole coated graphite oxide and graphene nanosheets as catalyst support materials for fuel cells, Fullerenes, Nanotubes and, Carbon Nanostruct. 21 (2013) 233–247.
[15] C. Zhou, J.A. Szpunar, X. Cui, Synthesis of Ni/graphene nanocomposite for hydrogen storage, ACS Appl. Mater. Interfaces 8 (2016) 15232–15241.
[16] A. Ngqalakwezi, D. Nkazi, G. Seifert, T. Ntho, Effects of reduction of graphene oxide on the hydrogen storage capacities of metal graphene nanocomposite, Catal. Today 358 (2020) 338–344.
[17] M. Kaur, K. Pal, An investigation for hydrogen storage capability of zirconia-reduced graphene oxide nanocomposite, Int. J. Hydrogen Energy 41 (2016) 21861–21869.
[18] Y. Wu, Y. Lin, A.A. Bol, K.A. Jenkins, F. Xia, D.B. Farmer, Y. Zhu, P. Avouris, High-frequency, scaled graphene transistors on diamond-like carbon, Nature 472 (2011) 74–78.
[19] A. Rezvani-Moghaddam, Z. Ranjbar, U. Sundararaj, A. Jannesari, A. Dashtdar, Edge and basal functionalized graphene oxide nanosheets: two different behavior in improving electrical conductivity of epoxy nanocomposite coatings, Prog. Org. Coating 172 (2022) 107143, https://doi.org/10.1016/j.porgcoat.2022.107143.
[20] A. Rezvani Moghaddam, M. Kamkar, Z. Ranjbar, U. Sundararaj, A. Jannesari, B. Ranjbar, Tuning the network structure of graphene/epoxy nanocomposites by controlling edge/basal localization of functional groups, Ind. Eng. Chem. Res. 58 (2019) 21431–21440, https://doi.org/10.1021/acs.iecr.9b03607.
[21] A. Rezvani Moghaddam, Z. Ranjbar, U. Sundararaj, A. Jannesari, M. Kamkar, A novel electrically conductive water borne epoxy nanocomposite coating based on graphene: facile method and high efficient graphene dispersion, Prog. Org. Coating 136 (2019) 105223, https://doi.org/10.1016/j.porgcoat.2019.105223.
[22] R. Rafiei Hashjin, Z. Ranjbar, H. Yari, Modeling of electrical conductive graphene filled epoxy coatings, Prog. Org. Coating 125 (2018) 411–419, https://doi.org/10.1016/j.porgcoat.2018.09.030.
[23] A. Kausar, I. Ahmad, T. Zhao, O. Aldaghri, K.H. Ibnaouf, M.H. Eisa, Cutting-edge graphene nanocomposites with polythiophene—design, features and forefront potential, J. Compos. Sci. 7 (2023) 319, https://doi.org/10.3390/jcs7080319.
[24] J. Zhu, X. Zhang, N. Haldolaarachchige, Q. Wang, Z. Luo, J. Ryu, D.P. Young, S. Wei, Z. Guo, Polypyrrole metacomposites with different carbon nanostructures, J. Mater. Chem. 22 (2012) 4996, https://doi.org/10.1039/c2jm14020a.
[25] S.M. Imran, Y. Kim, G.N. Shao, M. Hussain, Y. Choa, H.T. Kim, Enhancement of electroconductivity of polyaniline/graphene oxide nanocomposites through in situ emulsion polymerization, J. Mater. Sci. 49 (2014) 1328–1335, https://doi.org/10.1007/s10853-013-7816-5.
[26] M. Uz, S.K. Mallapragada, Conductive polymers and hydrogels for neural tissue engineering, J. Indian Inst. Sci. 99 (2019) 489–510, https://doi.org/10.1007/s41745-019-00126-8.
[27] S.K. Simotwo, C. DelRe, V. Kalra, Supercapacitor electrodes based on high-purity electrospun polyaniline and polyaniline–carbon nanotube nanofibers, ACS Appl. Mater. Interfaces 8 (2016) 21261–21269, https://doi.org/10.1021/acsami.6b03463.
[28] E. Akbarinezhad, M. Sabouri, Synthesis of exfoliated conductive polyaniline–graphite nanocomposites in supercritical CO2, J. Supercrit. Fluids 75 (2013) 81–87, https://doi.org/10.1016/j.supflu.2012.12.025.
[29] L. Groenendaal, F. Jonas, D. Freitag, H. Pielartzik, J.R. Reynolds, Poly(3,4-ethylenedioxythiophene) and its derivatives: past, present, and future, Adv. Mater. 12 (2000) 481–494, https://doi.org/10.1002/(SICI)1521-4095(200004)12:7<481::AID-ADMA481>3.0.CO;2-C.
[30] G.H. Kim, D.H. Hwang, S.I. Woo, Thermoelectric properties of nanocomposite thin films prepared with poly (3, 4-ethylenedioxythiophene) poly (styrenesulfonate) and graphene, Phys. Chem. Chem. Phys. 14 (2012) 3530–3536.
[31] F.-P. Du, N.-N. Cao, Y.-F. Zhang, P. Fu, Y.-G. Wu, Z.-D. Lin, R. Shi, A. Amini, C. Cheng, PEDOT:PSS/graphene quantum dots films with enhanced thermoelectric properties via strong interfacial interaction and phase separation, Sci. Rep. 8 (2018) 6441, https://doi.org/10.1038/s41598-018-24632-4.
[32] E. Hosseini, V. Ozhukil Kollath, K. Karan, The key mechanism of conductivity in PEDOT:PSS thin films exposed by anomalous conduction behaviour upon solvent-doping and sulfuric acid post-treatment, J. Mater. Chem. C 8 (2020) 3982–3990, https://doi.org/10.1039/C9TC06311K.
[33] J. Ouyang, "Secondary doping" methods to significantly enhance the conductivity of PEDOT:PSS for its application as transparent electrode of optoelectronic devices, Displays 34 (2013) 423–436, https://doi.org/10.1016/j.displa.2013.08.007.
[34] X. Liu, X.-L. Shi, L. Zhang, W.-D. Liu, Y. Yang, Z.-G. Chen, One-step post-treatment boosts thermoelectric properties of PEDOT:PSS flexible thin films, J. Mater. Sci. Technol. 132 (2023) 81–89, https://doi.org/10.1016/j.jmst.2022.05.047.

[35] S. Khasim, A. Pasha, M. Lakshmi, P. Chellasamy, M. Kadarkarai, A.A.A. Darwish, T. A. Hamdalla, S.A. Al-Ghamdi, S. Alfadhli, Post treated PEDOT-PSS films with excellent conductivity and optical properties as multifunctional flexible electrodes for possible optoelectronic and energy storage applications, Opt. Mater. 125 (2022) 112109, https://doi.org/10.1016/j.optmat.2022.112109.
[36] H. Zhou, M.H. Chua, Q. Zhu, J. Xu, High-performance PEDOT:PSS-based thermoelectric composites, Compos. Commun. 27 (2021) 100877, https://doi.org/10.1016/j.coco.2021.100877.
[37] R. Hegde, B. Pramanick, Polymer nanocomposite thin films prepared using single- and multi-walled carbon nanotubes for flexible electronics, J. Mater. Sci. Mater. Electron. 34 (2023) 1012, https://doi.org/10.1007/s10854-023-10457-z.
[38] M.S.A. Bhuyan, M.N. Uddin, M.M. Islam, F.A. Bipasha, S.S. Hossain, Synthesis of graphene, Int. Nano Lett. 6 (2016) 65–83.
[39] Y. Sun, W. Liu, I. Hernandez, J. Gonzalez, F. Rodriguez, D. Dunstan, C. Humphreys, 3D strain in 2D materials: to what extent is monolayer graphene graphite? Phys. Rev. Lett. 123 (2019) 135501.
[40] S. Stankovich, D.A. Dikin, R.D. Piner, K.A. Kohlhaas, A. Kleinhammes, Y. Jia, Y. Wu, S.T. Nguyen, R.S. Ruoff, Synthesis of graphene-based nanosheets via chemical reduction of exfoliated graphite oxide, Carbon 45 (2007) 1558–1565.
[41] D. Li, M.B. Müller, S. Gilje, R.B. Kaner, G.G. Wallace, Processable aqueous dispersions of graphene nanosheets, Nat. Nanotechnol. 3 (2008) 101–105, https://doi.org/10.1038/nnano.2007.451.
[42] X. Wang, L. Zhi, K. Müllen, Transparent, conductive graphene electrodes for dye-sensitized solar cells, Nano Lett. 8 (2008) 323–327, https://doi.org/10.1021/nl072838r.
[43] H.A. Becerril, J. Mao, Z. Liu, R.M. Stoltenberg, Z. Bao, Y. Chen, Evaluation of solution-processed reduced graphene oxide films as transparent conductors, ACS Nano 2 (2008) 463–470, https://doi.org/10.1021/nn700375n.
[44] E.Y. Pisarevskaya, O. Efimov, Graphene oxide as a basis for molecular design, Protect. Met. Phys. Chem. Surface 55 (2019) 468–472.
[45] F. Amato, G. Perini, G. Friggeri, A. Augello, A. Motta, L. Giaccari, R. Zanoni, M. De Spirito, V. Palmieri, A.G. Marrani, Unlocking the stability of reduced graphene oxide nanosheets in biological media via use of sodium ascorbate, Adv. Mater. Interfac. 10 (2023) 2300105.
[46] H. Chang, G. Wang, A. Yang, X. Tao, X. Liu, Y. Shen, Z. Zheng, A transparent, flexible, low-temperature, and solution-processible graphene composite electrode, Adv. Funct. Mater. 20 (2010) 2893–2902.
[47] F. Soltani-kordshuli, F. Zabihi, M. Eslamian, Graphene-doped PEDOT:PSS nanocomposite thin films fabricated by conventional and substrate vibration-assisted spray coating (SVASC), Eng. Sci. Technol. Int. J. 19 (2016) 1216–1223, https://doi.org/10.1016/j.jestch.2016.02.003.
[48] P.C. Mahakul, K. Sa, B. Das, B.V.R.S. Subramaniam, S. Saha, B. Moharana, J. Raiguru, S. Dash, J. Mukherjee, P. Mahanandia, Preparation and characterization of PEDOT:PSS/reduced graphene oxide–carbon nanotubes hybrid composites for transparent electrode applications, J. Mater. Sci. 52 (2017) 5696–5707, https://doi.org/10.1007/s10853-017-0806-2.
[49] Y.G. Seol, T.Q. Trung, O.-J. Yoon, I.-Y. Sohn, N.-E. Lee, Nanocomposites of reduced graphene oxide nanosheets and conducting polymer for stretchable transparent conducting electrodes, J. Mater. Chem. 22 (2012) 23759–23766, https://doi.org/10.1039/c2jm33949h.
[50] A. Giuri, S. Masi, S. Colella, A. Listorti, A. Rizzo, A. Liscio, E. Treossi, V. Palermo, G. Gigli, C. Mele, C. Esposito Corcione, GO/PEDOT:PSS nanocomposites: effect of different dispersing agents on rheological, thermal, wettability and electrochemical properties, Nanotechnology 28 (2017), https://doi.org/10.1088/1361-6528/aa6517.
[51] R. Striani, E. Stasi, A. Giuri, M. Seiti, E. Ferraris, C. Esposito Corcione, Development of an innovative and green method to obtain nanoparticles in aqueous solution from carbon-based waste ashes, Nanomaterials 11 (2021) 577, https://doi.org/10.3390/nano11030577.
[52] M. Zhang, W. Yuan, B. Yao, C. Li, G. Shi, Solution-processed PEDOT: PSS/graphene composites as the electrocatalyst for oxygen reduction reaction, ACS Appl. Mater. Interfaces 6 (2014) 3587–3593.
[53] A. Giuri, S. Masi, S. Colella, A. Listorti, A. Rizzo, A. Kovtun, S. Dell'Elce, A. Liscio, C. Esposito Corcione, Rheological and physical characterization of PEDOT: PSS/graphene oxide nanocomposites for perovskite solar cells, Polym. Eng. Sci. 57 (2017) 546–552, https://doi.org/10.1002/pen.24554.
[54] W. Hong, Y. Xu, G. Lu, C. Li, G. Shi, Transparent graphene/PEDOT–PSS composite films as counter electrodes of dye-sensitized solar cells, Electrochem. Commun. 10 (2008) 1555–1558.
[55] C. Sriprachuabwong, C. Karuwan, A. Wisitsorrat, D. Phokharatkul, T. Lomas, P. Sritongkham, A. Tuantranont, Inkjet-printed graphene-PEDOT: PSS modified screen printed carbon electrode for biochemical sensing, J. Mater. Chem. 22 (2012) 5478–5485.
[56] A. Vittore, M.R. Acocella, G. Guerra, Edge-oxidation of graphites by hydrogen peroxide, Langmuir 35 (2019) 2244–2250.
[57] Available online:, Data Sheet, 2023 https://www.heraeus.com/en/hep/products_hep/clevios_selector/productdetail/Clevios%E2%84%A2%20PH%201000.html. (Accessed 7 November 2023).
[58] C.E. Corcione, F. Freuli, A. Maffezzoli, The aspect ratio of epoxy matrix nanocomposites reinforced with graphene stacks, Polym. Eng. Sci. 53 (2013) 531–539.
[59] J. Kim, J. Jung, D. Lee, J. Joo, Enhancement of electrical conductivity of poly (3, 4-ethylenedioxythiophene)/poly (4-styrenesulfonate) by a change of solvents, Synth. Met. 126 (2002) 311–316.
[60] S. Jönssona, J. Birgerson, X. Crispin, G. Greczynski, W. Osikowicz, A.D. van der Gonc, W. Salaneck, M. Fahlman, The effects of solvents on the morphology and sheet resistance in poly (3, 4-ethylenedioxythiophene)–polystyrenesulfonic acid (PEDOT–PSS) films, Synth. Met. 139 (2003) 1.
[61] J. Ouyang, Q. Xu, C.-W. Chu, Y. Yang, G. Li, J. Shinar, On the mechanism of conductivity enhancement in poly (3, 4-ethylenedioxythiophene): poly (styrene sulfonate) film through solvent treatment, Polymer 45 (2004) 8443–8450.
[62] A.M. Nardes, R.A. Janssen, M. Kemerink, A morphological model for the solvent-enhanced conductivity of PEDOT: PSS thin films, Adv. Funct. Mater. 18 (2008) 865–871.
[63] Y. Xia, J. Ouyang, Significant different conductivities of the two grades of poly (3, 4-ethylenedioxythiophene): poly (styrenesulfonate), Clevios P and Clevios PH1000, arising from different molecular weights, ACS Appl. Mater. Interfaces 4 (2012) 4131–4140.
[64] A.S. Alshammari, M. Shkunov, S.R.P. Silva, Inkjet printed PEDOT:PSS/MWCNT nano-composites with aligned carbon nanotubes and enhanced conductivity, Phys. Rapid Res. Ltrs 8 (2014) 150–153, https://doi.org/10.1002/pssr.201308231.
[65] L.B. Valdes, Resistivity measurements on germanium for transistors, Proc. IRE 42 (1954) 420–427.
[66] F. Smits, Measurement of sheet resistivities with the four-point probe, Bell Syst. Tech. J. 37 (1958) 711–718.